Sonometric Study of the Normal Tricuspid Valve Annulus in Sheep

Matthew E. Hiro, Jerome Jouan, Matthew R. Pagel, Emmanuel Lansac[1], Khee Hiang Lim[2], Hou-Sen Lim[2], Carlos M. G. Duran

The International Heart Institute of Montana Foundation at St. Patrick Hospital and Health Sciences Center and The University of Montana, Missoula, Montana, USA

Present address: [1]University of La Pitié-Salpêtriere, Paris, France; [2]Nanyang Technological University, Singapore

Background and aim of the study: **Mitral valve dynamic changes during the cardiac cycle have been previously studied in sheep using sonomicrometry. The study aim was to analyze geometric changes of the normal tricuspid annulus in sheep using a similar methodology. This is most likely the first tricuspid valve study using high temporal resolution (200 Hz = 200 data points per second).**

Methods: **Thirteen crystals were implanted in seven sheep along the annulus (n = 6), at the tips of papillary muscles (n = 3), at the free edge of the leaflets (n = 3), and at the apex of the left ventricle (n = 1). Recordings (10 s) of crystal distances were used to create a three-dimensional (3D) coordinate system based on the least-squares plane of the annulus, and maximum and minimum values were calculated for length, area, and position in *xyz* coordinates.**

Results: **During the cardiac cycle, the tricuspid annulus area expanded 28.6 ± 3.6% with similar maximum expansions of each segment along the annulus: septal (10.4 ± 1.2%), anterior (13.0 ± 1.5%), and posterior (14.0 ± 1.6%). The annulus was saddle-shaped, with a circumferential expansion from elliptical at minimum area to more circular at maximum area. The time delay to maximum leaflet area and maximum papillary area occurred 83 ± 13 ms and 279 ± 30 ms respectively after maximum annulus area.**

Conclusion: **The tricuspid valve undergoes continual and complex geometric changes during the cardiac cycle. In addition, the annulus expands significantly due to similar increases in length of the septal and free wall segments. The annulus is not in a single plane, but is saddle-shaped. The expansion and contraction of the tricuspid valve complex is stepwise, and sequential from base to apex.**

The Journal of Heart Valve Disease 2004;13:452-460

Studies of the tricuspid valve have always lagged behind those of other cardiac valves because, when diseased, the valve's scant symptomatology and difficult diagnosis have minimized its real frequency and importance. Recent advances in echocardiography have revealed a higher than expected incidence of tricuspid insufficiency, and less than perfect results of its surgical management. This is particularly significant in functional regurgitation where, as with the mitral valve, late recurrence of the insufficiency is frequent. These unsatisfactory results call for a reappraisal of surgical techniques that in the past might have been based on an incomplete knowledge of the normal and pathological functional anatomy of the tricuspid valve.

Although dynamic changes of the aortic (1,2) and mitral (3-8) valves have been extensively studied in sheep using sonomicrometry, no similar studies have been reported for the tricuspid valve. The aim of the present study was to analyze the geometric changes that occur in the normal tricuspid valve during the cardiac cycle, using experience gained with sonomicrometry studies of the aortic and mitral valves.

Materials and methods

Animals

Seven adult sheep of mean (± SEM) bodyweight 69 ± 9 kg were used in these studies. Each animal underwent implantation of 13 ultrasonic crystals on the tricuspid valve using cardiopulmonary bypass (CPB) (pump time 135 ± 4 min; cross-clamp time 88 ± 2 min).

All animals received humane care in compliance with the principles of the Animal Welfare Act, the

Presented at the Second Biennial Meeting of the Society for Heart Valve Disease, 28th June-1st July, Palais des Congrès, Paris, France

Address for correspondence:
Carlos M. G. Duran MD, PhD, The International Heart Institute of Montana, 554 W. Broadway, Missoula, MT 59802, USA
e-mail: duran@saintpatrick.org

Guide for Care and Use of Laboratory Animals from the United States Department of Agriculture, and the Institutional Animal Care and Use Committee of The University of Montana.

Surgical protocol

Anesthesia was induced with intravenous ketamine (1.0 mg/kg) and propofol (4.0 mg/kg), and maintained with endotracheal isofluorane (1.5-2.5%). The electrocardiogram (ECG) was continuously monitored during surgery. Artificial ventilation was achieved with a volume-regulated respirator (North American Drager, Telford, PA, USA) supplemented with oxygen at 2 l/min.

The heart was exposed with a standard left thoracotomy through the fourth intercostal space and a T-shaped incision of the pericardium, and suspended in the pericardial cradle. The ascending aorta (#16 Fr), inferior vena cava (#32 Fr), and superior vena cava (#23 Fr) were cannulated, and CPB was instituted. A left ventricular vent line was inserted in the apex. The ascending aorta was then cross-clamped, followed by infusion of cold crystalloid cardioplegia into the aortic root.

In order to study the tricuspid valve complex, 13 ultrasonic crystals (Sonometrics Corporation, London, Ontario, Canada) were implanted through a right atriotomy. To avoid interoperator variability, the same surgeon placed all crystals. The 2-mm ultrasonic crystals were placed and secured with 5-0 polypropylene sutures. Crystals were located along the tricuspid annulus (n = 6) at the anteroseptal (A-S), anteroposterior (A-P) and posteroseptal (P-S) commissures, and at the relative midpoint of the base of the septal (S), anterior (A) and posterior (P) leaflets (Fig. 1). Similar 2-mm crystals were placed inside the right ventricle (n = 3) on the tips of the septal (Spm), anterior (Apm) and posterior (Ppm) papillary muscles. Smaller, 0.7-mm crystals (n = 3) were sutured to the free edge of the septal (SL), anterior (AL) and posterior (PL) leaflets. The electrodes of crystals on the annulus and leaflets were exteriorized through the right atriotomy, and the electrodes of crystals on the papillary muscles were exteriorized through the right ventricular wall. One crystal was sutured to the apex of the left ventricle to be used as a reference crystal. High-fidelity, catheter-tipped pressure transducers (model 510; Millar Instruments, Houston, TX, USA) were placed within the lumen of the pulmonary artery and in the right ventricle. A transonic flowmeter ring (Transonic Systems, Inc., Ithaca, NY, USA) was placed on the pulmonary trunk.

Experimental design

The study was conducted as an ovine, acute, anesthetized, open-chest and open pericardium model. After discontinuing CPB, and after the animal had been verified as hemodynamically stable (≥15 min), crystal distances were recorded along with right ventricular pressure, pulmonary trunk pressure and pulmonary artery flow. All recordings were performed at 200 Hz (one data point per 5 ms). Epicardial two-dimensional (2D) echocardiography with color Doppler was used to assess the competence and anatomy of the tricuspid valve. At the end of the experiment, the heart was arrested by lethal injection of potassium chloride and explanted from the body cavity, whereupon the correct position of the crystals was checked.

Definition of anatomic regions

The tricuspid annulus was studied during the cardiac cycle by determining its area; three circumferential lengths corresponding to the annular insertion of each leaflet (septal: P-S to S to A-S; anterior: A-S to A to A-P; posterior: A-P to P to P-S), and two diameters corresponding to the minimum and maximum dimension of the annulus. The *xyz* coordinates (based on the least-squares coordinate system described below) of the annulus crystals determined the 3D shape of the tricuspid annulus. The papillary muscles were studied by determining the area, distance of each muscle to the

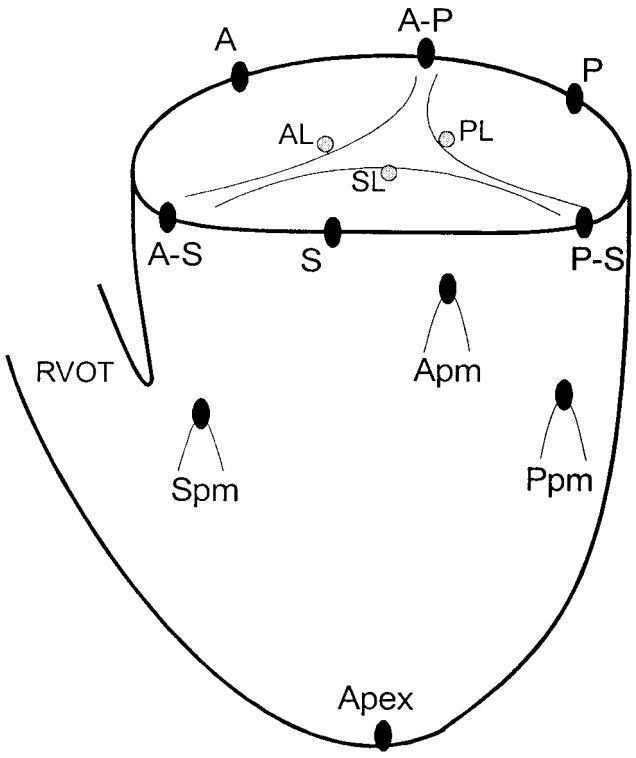

Figure 1: Location of sonometric crystals on the tricuspid valve complex. The black ovals represent 2.0-mm crystals; gray circles represent 0.7-mm crystals.

J Heart Valve Dis
Vol. 13. No. 1
January 2004

corresponding commissure (Spm to A-S, Apm to A-P and Ppm to P-S), and the angles between the papillary muscle to commissure line and the least-squares plane. The tricuspid leaflets were studied by determining the orifice area and the angles between the leaflet edge crystals and the least-squares plane.

Data acquisition and calculation of tricuspid deformations

Sonometrics Digital Ultrasonic Measurement System TRX Series (Sonometrics Corp.) 2-mm and 0.7-mm transmitter/receiver crystals were used to measure displacements. A post-processing program (Sonometrics Corp.) was used to examine each individual length tracing between crystals. All distances and pressures were synchronized with the ECG and recorded at the same timeline on the same screen using the Sonometrics system. Another post-processing program (SonoXYZ; Sonometrics Corp.) was then used to generate distance measurements between all crystals. The distances were used to create a 3D coordinate system based on the least-squares plane of the annulus using MATLAB (The Math Works, Inc., Natick, MA, USA). The distances were first used to define an arbitrarily placed Cartesian coordinate system. The coordinate system was then shifted to the tricuspid annulus to establish a meaningful reference frame as previously described by Gorman et al. (5). The centroid of the annulus crystals was calculated and set as the origin of the coordinate system. The approximate plane of the annulus was determined by least-squares regression of the annulus crystal coordinates and was set as the *x-y* plane. The positive *z*-axis was aligned normal to the least-squares plane opposite the direction of blood flow. The *x-z* plane was directed through the P-S crystal. The *x-z* plane and the least squares *x-y* plane thus defined the *x*-axis. Finally, the *y*-axis was chosen orthogonal to positive *x* and positive *z* in a right-handed coordinate system. The resulting system represented an approximation of the apicobasal direction (*z*-axis), the anterior-posterior direction (*x*-axis), and medial-lateral direction (*y*-axis) (Fig. 2).

Lagrangian strain (9) was used to define deformation of the tricuspid valve from minimum to maximum. The tricuspid annulus area was calculated by the addition of six triangles, each containing two annulus crystals projected into the least-squares plane and the centroid, and calculated using Heron's formula (10). The eccentricity of the tricuspid annulus was defined as the ratio of the minor axis (minimum dimension) to the major axis (maximum dimension) of the tricuspid annulus. The papillary area and leaflet area were calculated from the triangle formed from the three corresponding crystals using Heron's formula. The leaflet angles were also calculated using the following technique. First, a vector was constructed between the crystal at the midpoint of the base of the leaflet on the annulus and the crystal at the leaflet's edge. This vector was then projected into a radial plane defined by the radius from the centroid to the annulus midpoint crystal perpendicular to the *z*-axis. The angle between the projected vector and the least-squares plane was measured (Fig. 3). The papillary muscle angles were calculated using a vector from the papil-

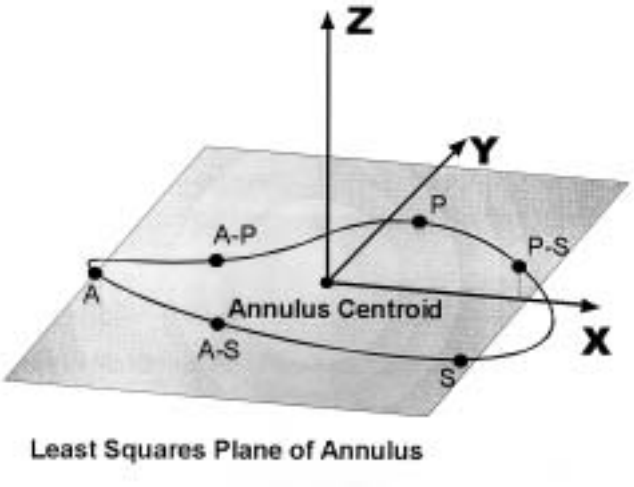

Figure 2: Schematic of the coordinate system developed from the least-squares plane of the annulus. The coordinate system is oriented with the x-axis in the direction of posteroseptal (P-S) commissure and with the z-axis opposite the direction of blood flow (see text).

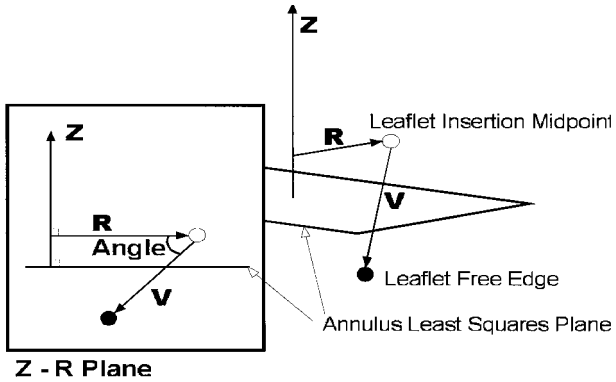

Figure 3: Schematic demonstrating the projection method used to calculate the angles formed by the least-squares plane of the annulus and the leaflet edge and papillary crystals. For the leaflet opening angle, the white marker represents a crystal at the midpoint of leaflet insertion and the black marker represents a leaflet free edge crystal. For the papillary muscle angle, the white marker represents a crystal at a commissure and the black marker represents a papillary muscle crystal (see text). The angle is measured between R and V in the Z-R plane.

lary crystal and the corresponding annular commissure (septal: Spm to A-S, anterior: Apm to A-P, posterior: Ppm to P-S) and the same projection method described above.

Each length and area was described by the minimum value, the maximum value, and the percentage of expansion with reference to the minimum and maximum. The shape of the tricuspid annulus was determined by the 3D coordinates of the annulus crystals at maximum annulus area and minimum annulus area. Each angle was described by the minimum value, the maximum value, and the change between minimum and maximum value. The timing of relative maxima of the annulus, leaflets, and papillary muscles was determined by computing the time delay between each of the maximum peaks.

Measurements and statistical analysis

After close examination of the data, three consecutive heartbeats with the least amount of noise were chosen for analysis. The summary statistics were reported as mean ± SEM. Changes in distance were tested by conducting a two-tailed *t*-test for paired comparisons with a significance level $p \leq 0.05$. All statistical analysis was carried out using Excel (Microsoft Corporation, Seattle, WA, USA).

Results

Model characteristics

At the time of recording, the hemodynamic conditions were as follows: heart rate 99 ± 6 beats per min; arterial pressure 67/40 ± 2/3 mmHg; stroke volume 33 ± 2 ml; and cardiac output 2.9 ± 0.4 l/min (Table I). All valves were competent on epicardial echocardiography. At necropsy, all crystals were in the correct position in six animals. In one sheep, two papillary muscle crystals were incorrectly placed, with both Spm and Apm being placed on the septum. Hence, all calculations in this animal which were dependent on the correct positioning of these two crystals were excluded, whereas calculations involving the annulus crystals were included.

Table I: Hemodynamic parameters during recordings for seven sheep.

Hemodynamic parameters	Mean ± SEM
Body weight (kg)	69 ± 9
Systolic arterial pressure (mmHg)	67 ± 2
Diastolic arterial pressure (mmHg)	40 ± 3
Systolic right ventricular pressure (mmHg)	26 ± 1
Diastolic right ventricular pressure (mmHg)	1 ± 1
Systolic pulmonary artery pressure (mmHg)	20 ± 1
Diastolic pulmonary artery pressure (mmHg)	11 ± 1
Stroke volume (ml)	33 ± 2
Cardiac output (l/min)	2.9 ± 0.4
Heart rate (beats/min)	99 ± 6

Tricuspid annulus expansion

The tricuspid valve area and perimeter were calculated in the least-squares plane to represent only cross-sectional area and length changes. No vertical (apicobasal) component was considered in these calculations. The annulus expanded in the least-squares plane from 4.8 ± 0.8 cm^2 to 6.1 ± 0.9 cm^2, an expansion of 28.6 ± 3.6% (reduction of 21.9 ± 2.2%). The segmental perimeter expansion was similarly computed in the least-squares plane along the insertion of the septal, anterior and posterior leaflets. The expansion of the base of each leaflet was similar but not equal for the septal (10.5 ± 1.2%), anterior (13.0 ± 1.5%) and posterior (14.0 ± 1.6%) leaflets (Table II).

Tricuspid annulus shape

The shape of the tricuspid annulus was determined by the 3D coordinates of each annulus crystal at minimum and maximum annulus area (Table III). The saddle shape of the annulus was defined by the height (*z*) of each crystal above or below the least-squares plane. The resultant averages determined a saddle oriented with relative maxima corresponding to crystal P and crystals A-S and A with local minima at A-P and P-S (Fig. 4).

The shape of the annulus in the *x-y* plane (Table III) can be seen at minimum and maximum area in Figure 5. The eccentricity of the annulus changed from 0.45 ± 0.05 to 0.55 ± 0.05. Therefore, at all times during the

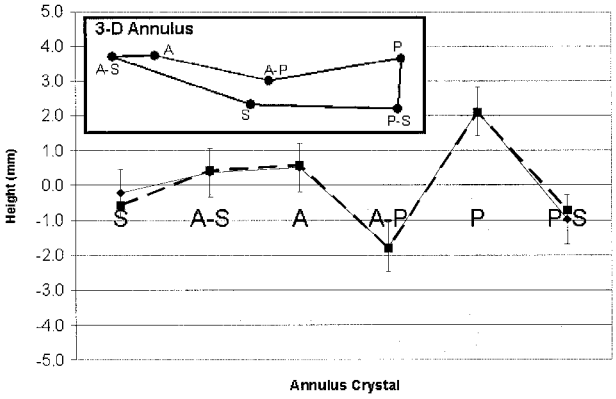

Figure 4: Saddle shape of the tricuspid annulus based on the height of the annulus crystals above or below the least-squares plane for seven sheep at minimum (dashed line) and maximum (solid line) annulus area. The error bars represent the largest SEM (= 0.7 mm) for the z-coordinate of all annulus crystals. The insert shows the positions of the annulus crystals in three dimensions.

J Heart Valve Dis
Vol. 13. No. 1
January 2004

Table II: Length data for tricuspid annulus (n = 7) and distances from papillary muscle to the corresponding commissure on the annulus (n = 6).

Measurement	Minimum (mm)	Maximum (mm)	Expansion (%)
Septal length	34.0 ± 3.5	38.3 ± 3.4	10.4 ± 1.2
Anterior length	20.4 ± 2.1	26.5 ± 2.3	13.0 ± 1.5
Posterior length	30.4 ± 2.4	34.4 ± 2.5	14.0 ± 1.6
Spm to A-S	16.2 ± 2.4	18.8 ± 2.5	20.6 ± 9.2
Apm to A-P	19.4 ± 1.3	21.8 ± 1.8	12.6 ± 6.9
Ppm to P-S	17.8 ± 1.4	21.0 ± 1.4	19.5 ± 8.2

The length along the annulus corresponds to the perimeter in the least-squares plane of the insertion of each leaflet. Measurements of distances from papillary muscle tip to annulus are excluded in one sheep.

cardiac cycle, the annulus had an elliptical shape and became slightly more circular during periods of maximum area and perimeter.

Leaflet opening

The opening of the tricuspid valve was determined from the area of the triangle designated by the three crystals on the leaflet edges (SL, AL, PL). This area expanded from a minimum of 0.3 ± 0.1 cm^2 to maximum of 1.6 ± 0.4 cm^2.

The angle formed by the leaflets and the least-squares plane was calculated in the radial plane (see Fig. 3). The angle formed by each leaflet edge in the corresponding plane was used as a measure of excursion of each leaflet. At maximum excursion, SL opened the least (56.9 ± 4.2º) with respect to the least-squares plane compared with AL (96.0 ± 13.6º, p = 0.034) and PL (90.8 ± 11.5º, p = 0.018) (Table IV). The change in angle from minimum to maximum of SL was also considerably smaller (+29.8 ± 4.0º) than AL (+58.5 ± 14.5º, p = 0.017) and PL (+48.8 ± 7.5º, p = 0.066).

Motion of the papillary muscles

The triangular area formed by the papillary muscles expanded from 2.7 ± 0.5 cm^2 to 3.6 ± 0.6 cm^2 (+37.3 ± 8.5%). The angles formed by the papillary muscles were perpendicular to the annulus LSP at maximum excursion for Spm (94.3 ± 8.8º), Apm (92.6 ± 8.3º), and Ppm (90.4 ± 5.9º) (Table IV). However, the change in angle was larger for Apm (+24.8 ± 5.0º) compared with Spm (+13.9 ± 4.0º, p = 0.117) and Ppm (+9.5 ± 1.1º, p = 0.039). The apical distance between the annulus and each papillary muscle was also compared. The percentage change from minimum to maximum was smaller for Apm (12.6 ± 6.9%) compared with Spm (20.6 ± 9.2%, p = 0.046) and Ppm (19.5 ± 8.2%, p = 0.044) (see Table II).

Timing of relative expansions

To compare the timing of the expansion of the annulus, leaflets and papillary muscles, the area data for each system were displayed on the same graph for three beats (Fig. 6). Because the area of the papillary

Table III: Three-dimensional coordinates for the annulus crystals (n = 7) and papillary crystals (n = 6) at maximum and minimum annulus area (in mm).

Crystal	Max X	Min X	Change X	Max Y	Min Y	Change Y	Max Z	Min Z	Change Z
S	7.5 ± 1.1	8.0 ± 1.3	-0.4 ± 0.4	-11.0 ± 1.4	-8.5 ± 1.6	-2.4 ± 0.6	-0.2±0.4	-0.6 ± 0.6	0.3 ± 0.4
AS	-12.6 ± 1.8	-11.7 ± 1.4	-0.9 ± 0.5	-10.6 ± 1.0	-9.3 ± 1.1	-1.3 ± 0.2	0.4 ± 0.5	0.4 ± 0.4	-0.1 ± 0.3
A	-17.2 ± 1.4	-16.5 ± 1.1	-0.7 ± 0.4	2.8 ± 0.9	2.6 ± 1.3	0.3 ± 0.5	0.5 ± 0.6	0.6 ± 0.5	-0.1 ± 0.3
A-P	-7.9 ± 0.8	-7.9 ± 0.8	-0.0 ± 0.3	8.5 ± 0.7	7.7 ± 1.0	0.8 ± 0.4	-1.8 ± 0.4	-1.8 ± 0.5	0.0 ± 0.3
P	8.9 ± 2.1	7.7 ± 1.9	1.2 ± 0.4	10.2 ± 1.4	7.6 ± 1.4	2.6 ± 0.4	2.1 ± 0.7	2.1 ± 0.6	0.0 ± 0.3
PS	21.3 ± 1.7	20.4 ± 1.5	0.9 ± 0.3	-	-	-	-1.0 ± 0.4	-0.7 ± 0.5	-0.3 ± 0.2
Spm	-10.9 ± 1.5	-9.0 ± 1.8	-2.0 ± 0.5	-14.7±2.3	-10.8 ± 3.0	-3.9 ± 1.1	-14.0 ± 1.8	-14.8 ± 1.8	0.8 ± 0.6
Apm	-5.8 ± 3.8	-0.7 ± 3.0	1.0 ± 1.3	4.8 ± 3.8	8.3 ± 3.9	-3.5 ± 1.4	-19.3 ± 1.5	-19.3 ± 1.4	0.0 ± 0.8
Ppm	19.1 ± 1.4	18.1 ± 1.6	1.0 ± 1.2	4.7 ± 1.9	7.9±2.2	-3.2 ± 1.2	18.2 ± 1.2	-18.1 ± 1.4	-0.1 ± 0.5

The three Cartesian axes are approximations of three anatomic axes (see text). Crystal P-S has no value for the *y*-coordinate because the *x*-axis (*y* = 0) is defined along the projection of this crystal in the least-squares plane.

Table IV: Maximum and minimum angles formed by each leaflet edge crystal (n = 7) and papillary muscle crystal (n = 6) with respect to the least-squares plane of the annulus.

Dimension	Min angle (°)	Max angle (°)	Change (%)
S L	27.1 ± 3.6	56.9 ± 4.2	29.8 ± 4.0
AL	37.5 ± 10.8	96.0 ± 13.6	58.5 ± 14.5
PL	42.0 ± 9.6	90.8 ± 11.5	48.8 ± 7.5
Spm	80.4 ± 8.1	94.3 ± 8.8	13.9 ± 4.0
Apm	67.8 ± 7.9	92.6 ± 8.3	24.8 ± 5.0
Ppm	81.0 ± 5.5	90.4 ± 5.9	9.5 ± 1.1

Maximum and minimum values respectively correspond to the maximum outward and inward excursion of each crystal (method of calculation exposed in Figure 3).

muscles is used as a reference, the data from the sheep with misplaced papillary crystals were excluded. The maximum of each beat at each position was determined, and the time differences between maxima were compared. During the cardiac cycle, the maximum area of the leaflets occurred 83 ± 13 ms after maximum annulus area, and the maximum area of the papillary muscles occurred 279 ± 30 ms time steps after the maximum annulus area (Fig. 6). Therefore, it appears that the tricuspid valve complex expands and contracts in a stepwise fashion, from base to apex. The annulus expands first during the cardiac cycle and begins contracting while the leaflets are opening to maximum area (Fig. 6). At maximum excursion of the leaflets (i.e. maximum leaflet area), the annulus area has already completed 56.1 ± 8.3% of the total (100%) contraction from the maximum value to minimum value.

Discussion

Functional tricuspid regurgitation has been largely ignored with apparent impunity. When surgically treated, the results of different annuloplasties are unsatisfactory (11,12). Bhudia et al. (11) recently reviewed 790 patients who underwent a variety of tricuspid annuloplasty methods for functional tricuspid regurgitation. At eight years of follow up, severe regurgitation (grade 3 to 4+) was present in 15% to 37%

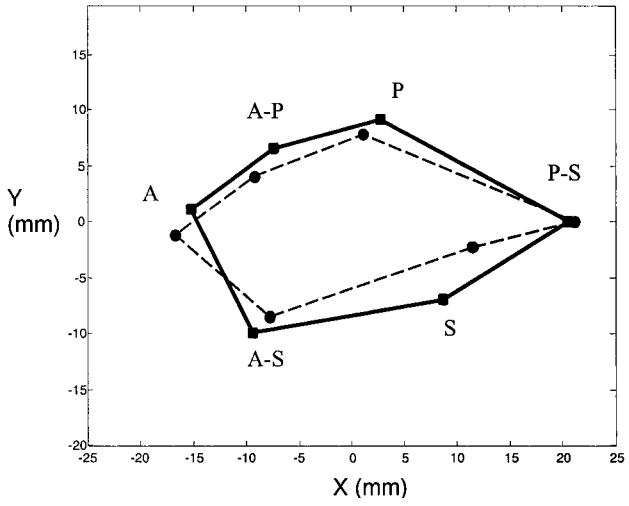

Figure 5: Shape of the annulus in the x-y (least squares) plane at minimum (dashed line) and maximum (solid line) area. From minimum to maximum area, the perimeter increases heterogeneously along the base of each leaflet, and the eccentricity increases as the annulus becomes more circular. Crystal P-S does not move along the y-axis because the projection of this crystal in the least-squares plane defines the x-axis (y = 0). The images are from one sheep.

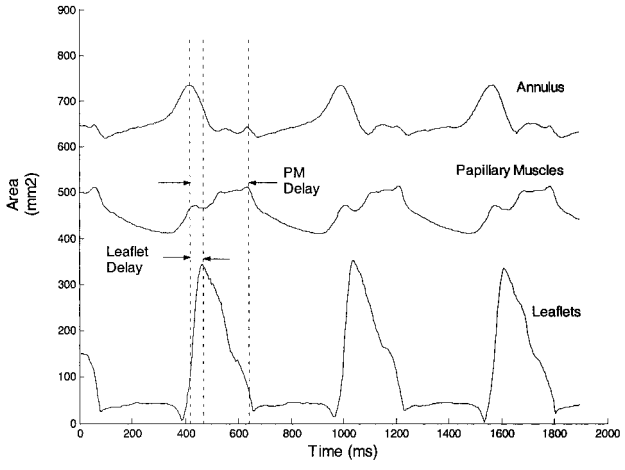

Figure 6: Timing of the maximum peak of annulus area, leaflet area, and papillary area over three beats for one sheep. The leaflet delay is the time (in ms) between maximum annulus area and maximum leaflet area. The papillary muscle (PM) delay is the time (in ms) between maximum annulus area and maximum papillary area.

of the patients according to the type of annuloplasty performed. A new look at the tricuspid valve based on a better understanding of its functional anatomy should stimulate the development of new approaches to its surgical repair.

The aim of the present study was to analyze the geometric changes of the normal tricuspid annulus during the cardiac cycle, using experience gained with sonomicrometry studies of the aortic and mitral valves (1-7). Thirteen crystals were placed around the tricuspid annulus, tips of the three papillary muscles, free edges of the three leaflets, and the left ventricular apex. The sonometric crystals are piezoelectric transducers that measure intercrystal distances every 5 ms with an accuracy of 0.0248 mm. The high temporal resolution and spatial precision allows marker positions to be recorded in three dimensions at a frequency of 200 per second.

Analysis of the data obtained confirmed those of Tsakiris and associates (13), who originally showed in the dog that the tricuspid annulus changed its size and shape continuously during the cardiac cycle. At low heart rates, the annulus orifice area reached a maximum reduction of 39%. In an echocardiographic study of normal humans, Tei et al. (14) showed a maximum reduction of 33%, and in the present study the reduction was 21.9 ± 2.2%. This reduction in annulus orifice was understood to be due to a selective shortening of the free wall portions (13). However, contrary to expectations, the length of insertion of the septal leaflet changed almost as much as the insertion of the anterior and posterior leaflets (10.4 ± 1.2% versus 13.0 ± 1.5% versus 14.0 ± 1.6%).

The normal tricuspid annulus is usually depicted as pear-shaped, with its narrower end close to the anteroseptal commissure and its wider end corresponding to the midpoint of the posterior leaflet. As described by Deloche et al. (15) in the post-mortem human heart, the present authors also observed this shape in the pressurized post-mortem sheep heart, though in the present in-vivo model the opposite shape was found. The narrow end of the pear-shaped annulus corresponded to the posteroseptal commissure (Fig. 5).

The tricuspid annulus has a distinctly non-planar shape (Fig. 4). At minimum and maximum area of the annulus, the highest points of the saddle coincided with the mid-posterior crystal (P) and the mid-anterior (A) and anteroseptal (A-S) crystals, with local minima at the anteroposterior commissure (A-P) and posteroseptal commissure (P-S) crystals. The mechanical advantage of the saddle shape of the tricuspid annulus is unknown, but in the case of the mitral valve annulus, such a shape has been shown to reduce valve stress (16).

The excursion of the three leaflets was measured as the angle between the free edge and the least-squares plane of the annulus. The free edge of the septal leaflet changed by 29.8 ± 4.0° between its open and closed positions, while the anterior and posterior leaflet crystals moved 58.5 ± 14.5° ($p = 0.066$) and 48.8 ± 7.5° ($p = 0.017$), respectively (Table IV). This normal, smaller septal excursion might explain the finding of a septal leaflet plastered against the septum, which is often seen during surgery for severe functional regurgitation.

The location of the papillary muscles in relation to the tricuspid annulus was also explored. The angles between the tips of each papillary muscle and the least-squares plane of the annulus were calculated from maximum to minimum excursion. As expected, all three papillary muscles moved closer together during valve closure and separated during valve opening (Fig. 6). The anterior papillary crystal showed a maximum lateral displacement of 24.8 ± 5.0°, while the septal and posterior muscles changed by 13.9 ± 4.0° ($p = 0.117$) and 9.5 ± 1.1° ($p = 0.039$), respectively (Table IV). At maximum displacement, all three papillary muscles were within the perimeter of the annulus in the *x-y* plane with angle values close to 90° (Table IV). These relationships are bound to be significantly altered in functional tricuspid regurgitation. Recently, Otsuji et al. (17) showed that besides annular dilatation, the main mechanism of functional mitral regurgitation is tethering of the mitral leaflets by lateral and apical displacement of the papillary muscles. The mechanism of functional tricuspid regurgitation may follow a similar pattern.

The timing of expansion of the different structures of the tricuspid valve reveals the complexity of mechanisms involved in the opening and closing of the valve. The present preliminary data show a stepwise and sequential expansion and contraction pattern of the components of the tricuspid valve (Fig. 6). During the cardiac cycle, the annulus area reached maximum expansion first, followed by maximum leaflet expansion, and next by maximum papillary muscle expansion at 83 ± 13 ms and 279 ± 30 ms, respectively. At maximum leaflet area, the annulus area had already completed 56.1 ± 8.3% of the total (100%) contraction from the maximum to minimum value.

All of these findings question the adequacy of all present annuloplasties that selectively reduce the portion of the annulus corresponding to the right ventricular free wall, assuming that the length of the septal portion of the annulus remains constant in health and disease. Also, the length of the base of the septal leaflet is used to determine the optimal size of the repaired annulus. These principles were derived from the mitral valve, where the fibrous intertrigonal segment

was considered stable and constant. However, recent sonometric findings in sheep in the present authors' laboratory have shown a normal 11.5% change in the intertrigonal distance (3), and necropsy data of controls and patients with ischemic and dilated cardiomyopathies have shown a 44% enlargement of the mitral intertrigonal distance (18). These facts might also question the use of open-band posterior annuloplasties that do not protect the septal area from further dilatation.

Rigid annuloplasty rings induce a permanent pear shape that does not correspond to the natural tricuspid annulus, and also interferes with its constant changes in shape during the cardiac cycle. The flat, single-plane, rigid ring also abolishes the normal saddle shape of the annulus.

These preliminary data reveal that the tricuspid is a complex and probably very efficient valvular mechanism with a geometry that changes continuously during the cardiac cycle. As in the case of the mitral valve, none of the structures of the tricuspid valve can be studied in isolation. It is hoped that better knowledge of the dynamic geometric changes of the normal tricuspid valve will promote understanding of the mechanisms responsible for its functional regurgitation.

Study limitations

These investigations should be understood as being a preliminary study on a subject that has been largely ignored, since no previous sonomicrometry study of the tricuspid valve has been identified. Because this is also the first tricuspid study to be completed in the authors' laboratory, several limitations exist. First, all data were acquired in an acute, anesthetized, open-chest animal model. Also, the deleterious effect of CPB and ischemia might have resulted in abnormal valve behavior. The high heart rate and depressed diastolic arterial blood pressure, as compared with pre-bypass measurements, might have altered tricuspid motion during the cardiac cycle. The pericardium was not closed during measurements, eliminating its restraining effect on the right ventricle. The pre- and afterload conditions at the time of data recording were not controlled, and most likely varied extensively between animals. As a result, only differences between maximum and minimum distances and angles were considered. Because the right ventricular and pulmonary artery pressure tracings were unreliable in five animals, no attempt was made to correlate the geometric changes with the events of the cardiac cycle. However, findings on the changes in annulus area were very similar to those reported elsewhere. In addition, the preliminary nature of these investigations, the complexity of the right ventricular movements, and the presence of a single left ventricular apical crystal deterred the authors from studying the right ventricular torsion that must play an important role in tricuspid dynamics. Variability in the precise location of the crystals must also be considered, though to minimize this problem all surgery was performed by the same individual. Likewise, the presence of crystals and attached electrodes is inherent to sonometric studies. The annulus and leaflet electrodes were exteriorized through the right atriotomy, and the papillary crystals through the right ventricular wall. No electrodes traversed the valve. Additionally, it must be emphasized that the findings in sheep are not necessarily applicable to the human situation. Although most dynamic valve studies have used an ovine model, species differences in tissue compliance and leaflet thickness might influence these results. Despite these limitations, the data described should be valid for advancing our understanding of the tricuspid valve and developing new surgical procedures.

Acknowledgements

The authors thank Kathleen Billington, Holly Meskimen, and Leslie Trail for the effort and support essential to the completion of these experiments, and Jill Roberts for her editorial assistance.

References

1. Lansac E, Lim HS, Shomura Y, et al. A four-dimensional study of the aortic root dynamics. Eur J Cardiothorac Surg 2002;22:497-503
2. Pang DC, Choo SJ, Luo HH, et al. Significant increase of aortic root volume and commissural area occurs prior to aortic valve opening. J Heart Valve Dis 2000;9:9-15
3. Lansac E, Lim KH, Shomura Y, et al. Dynamic balance of the aortomitral junction. J Thorac Cardiovasc Surg 2002;123:911-918
4. Gorman RC, McCaughan JS, Ratcliffe MB, et al. Pathogenesis of acute ischemic mitral regurgitation in three dimensions. J Thorac Cardiovasc Surg 1995;109:684-693
5. Gorman JH, III, Gupta KB, Streicher JT, et al. Dynamic three-dimensional imaging of the mitral valve and left ventricle by rapid sonomicrometry array localization. J Thorac Cardiovasc Surg 1996;112:712-726
6. Gorman JH, III, Gorman RC, Jackson BM, et al. Distortions of the mitral valve in acute ischemic mitral regurgitation. Ann Thorac Surg 1997;64:1026-1031
7. Gorman JH, III, Jackson BM, Gorman RC, Kelley ST, Gikakis N, Edmunds LH, Jr. Papillary muscle discoordination rather than increased annular area facilitates mitral regurgitation after acute posterior myocardial infarction. Circulation 1997;96(9 Suppl.):II124-II127

8. Jackson BM, Gorman JH, Moainie SL, et al. Extension of borderzone myocardium in postinfarction dilated cardiomyopathy. J Am Coll Cardiol 2002;40:1160-1167; discussion 1168-1171
9. Fung YC. Biomechanics Motion, Flow, Stress, and Growth. Springer-Verlag, New York, 1990:358
10. Pappas T. The Joy of Mathematics. 2nd edn. Wide World Publishing/Tetra, San Carlos, CA, 1989:62
11. Bhudia SK, McCarthy PM, Rajeswaran J, et al. Tricuspid Valve Repair: Durability and Risk Factors for Failure. 83rd Annual Meeting of the American Association of Thoracic Surgery May 4-7, 2003, Boston, MA, USA
12. Duran CM, Pomar JL, Colman T, Figueroa A, Revuelta JM, Ubago JL. Is tricuspid valve repair necessary? J Thorac Cardiovasc Surg 1980;80:849-860
13. Tsakiris AG, Mair DD, Seki S, Titus JL, Wood EH. Motion of the tricuspid valve annulus in anesthetized intact dogs. Circ Res 1975;36:43-48
14. Tei C, Pilgrim JP, Shah PM, Ormiston JA, Wong M. The tricuspid valve annulus: Study of size and motion in normal subjects and in patients with tricuspid regurgitation. Circulation 1982;66:665-671
15. Deloche A, Guerinon J, Fabiani JN, et al. [Anatomical study of rheumatic tricuspid valvulopathies. Applications to the critical study of various methods of annuloplasty]. Arch Mal Coeur Vaiss 1974;67:497-505 (in French)
16. Salgo IS, Gorman JH, III, Gorman RC, et al. Effect of annular shape on leaflet curvature in reducing mitral leaflet stress. Circulation 2002;106:711-717
17. Otsuji Y, Handschumacher MD, Schwammenthal E, et al. Insights from three-dimensional echocardiography into the mechanism of functional mitral regurgitation: Direct in vivo demonstration of altered leaflet tethering geometry. Circulation 1997;96:1999-2008
18. Hueb AC, Jatene FB, Moreira LF, Pomerantzeff PM, Kallas E, de Oliveira SA. Ventricular remodeling and mitral valve modifications in dilated cardiomyopathy: New insights from anatomic study. J Thorac Cardiovasc Surg 2002;124:1216-1224

Meeting discussion

DR. BLASE CARABELLO (Houston, Texas, USA): I feel certain that these are unique data. One problem, of course, is that while the mitral valve has, at least in part, lent itself to echocardiographic exploration, the tricuspid valve does not do so very well. So, what do you plan from here? Will you study sheep long term with pressure overload and ischemia? Having developed the baseline, there are now many very interesting explorations you can make.
DR. JOUAN: Yes, that's true.
DR. D. CRAIG MILLER (Stanford, California, USA): On your horizontal graph I couldn't quite detect the high point. Is it between the junction of the anterior and posterior leaflets, or is it in the middle of the anterior leaflet?
DR. JOUAN: It is in the middle of the posterior leaflet.
DR. MILLER: So the 3-D echo that led to the design of the Cosgrove-Edwards MC3 tricuspid ring is different? Not incorrect, but different. Is that so?
DR. JOUAN: Yes, it's different.
DR. MILLER: But that was human and this is sheep, so we cannot not say correct or incorrect - just different.
DR. JOUAN: Yes.
DR. MILLER: I think Toby designed his ring by validating with 3-D echo? I would expect the high point in humans to be right where the aortic valve starts - in the middle of the anterior?
DR. JOUAN: It's with respect to the least-square plane of the crystals.
DR. MILLER: Maybe that's what's throwing a curve ball in here.
DR. J. MICHAEL HASENKAM (Aarhus, Denmark): Did you make any validation of the impact of the transducers on the leaflets, or whether the transducers themselves had any influence on the freeness of the movement?
DR. JOUAN: Sonomicrometry has been validated as a good method for the mitral and aortic valves, and we only carried out an echocardiogram to check that there was no regurgitation. Otherwise, I don't really know - the movement by itself may change a little.